



OPEN Dynamic reconfiguration of multiobjective distribution networks considering the variation of load and DG using a novel LDEDBO algorithm

Yanmin Wu^{1,2}, Lu Wang^{1✉}, Zhenjie Wan¹, Jiaqi Liu¹, Dongpeng Fu³, Yanjun An¹ & Xiaofeng Zhang²

To address the challenges related to active power dissipation and node voltage fluctuation in the practical transformation of power grids in the field of new energy such as wind and photovoltaic power generation, an improved Dung Beetle Optimization Algorithm Based on a Hybrid Strategy of Levy Flight and Differential Evolution (LDEDBO) is proposed. This paper systematically addresses this issue from three aspects: firstly, optimizing the DBO algorithm using Chebyshev chaotic mapping, Levy flight strategy, and differential evolution algorithm; secondly, validating the algorithm's feasibility through real-time network reconfiguration at random time points within a 24-h period; and finally, applying the LDEDBO to address the dynamic reconfiguration problems of the IEEE-33 and IEEE-69 node bus. The simulation indicates that the power dissipation of the IEEE-33 node bus is decreased by 28.94% and the minimum node voltage is elevated from 0.9273 p.u to 0.9447 p.u after the reconstruction with LDEDBO. The power dissipation of the IEEE-69 node bus is reduced by 36.45%, and the minimum node voltage is increased from 0.9224 p.u to 0.9481 p.u. The LDEDBO enhances both the pace of convergence and the precision of the optimization model, leading to a superior solution for the switching combination.

Keywords Distribution network reconfiguration, LDEDBO algorithm, Optimization algorithm, Dynamic reconfiguration, Time-varying load

In 2022, the global energy landscape underwent a significant shift, with the carbon intensity of global power generation historically dropping to 436 gCO₂/kWh. Solar power generation increased by a substantial 24%, and wind power by 17%, making a crucial contribution to the clean and renewable energy sector¹. The new distribution grid seamlessly integrates clean energy with the power system. Simultaneously, the application of intelligent management technology further improves the efficiency and controllability of the energy system. Together, these transformations shape a clean and sustainable energy future. The restructuring of the distribution grid, as a key component of this paradigm shift, aims to redesign and optimize the distribution system to better accommodate the large-scale integration of clean energy².

When small power generation and storage devices (such as photovoltaic cells, wind generators, and energy storage cells.) are connected to the grid system as distributed generation (DG), they can cause voltage fluctuations, frequency distortion, and changes in power flow³. In this case, it is imperative to reconfigure the power grid by formulating the goal function and adjusting the state of the grid-connected switch and the segment switch⁴. Chandramohan et al.⁵ proposed the minimization of operating costs and the maximization of operational reliability as objective functions. Operating costs include the price of both active and reactive power, while operational reliability is achieved by minimizing total system outage costs. Additionally, Gözel et al.⁶ determined the optimal scale and location of DG by minimizing total power loss. Gupta et al.⁷ transformed various power quality and reliability objectives such as feeder power losses, system's nodal voltage deviations, system's average interruption frequency index, system's average interruption unavailability index, and unserved

¹College of Building Environment Engineering, Zhengzhou University of Light Industry, Zhengzhou 450002, China.

²College of Electric Engineering, Naval University of Engineering, Wuhan 430033, China. ³School of Accounting, Henan University of Engineering, Zhengzhou 451191, China. ✉email: 332222020890@zzuli.edu.cn

energy into a single objective function, which was then genetic algorithm is used to solve this single objective problem. Besides, several commonly used objective functions include minimum investment cost^{8,9}, minimum voltage stability index¹⁰, minimum load balancing index¹¹, among others.

However, the aforementioned studies primarily focus on the static reconfiguration problem at individual time points, unable to address the dynamic changes during the operation of the power system. Dynamic reconfiguration involves real-time monitoring and adjustments to the system state to adapt to the evolving operational conditions of the power system. This encompasses dynamic adjustments to load, power sources, and network topology to meet the real-time demands and fluctuations of the power system. Therefore, many researchers define distribution grid reconfiguration as a dynamic issue requiring real-time monitoring, system feedback, and efficient decision algorithms to ensure the smooth operation of the power system in a dynamic environment¹². Considering the inherent uncertainty associated with distributed photovoltaic (PV) systems, a recent study by Xu et al.¹³ introduced a novel multi-objective and robust optimization strategy aimed at maximizing the utilization of renewable energy resources. Besides, Pan and Wang et al.^{14,15} considered the restriction of load demand curve on network changing action, the reconstruction cycle is divided according to load monotonicity and amplitude variation. Li et al.¹⁶ constructed an ADN integrated optimization model considering photovoltaic, wind power, dynamic load and real-time electricity price. The MOSSA-based approach formulates an excellent optimization scheme with the highest power quality and the best energy and economic benefits.

Metaheuristic algorithms, due to their versatility and flexibility, have been widely applied in the field of power systems. For example, Senapati et al.¹⁷ proposed a novel intelligent control system based on the TS fuzzy algorithm to address power quality issues in power systems, such as voltage sags, voltage harmonics, nonlinear loads, and load imbalance, thereby improving the overall performance of the power system. Senapati et al.¹⁸ introduced a priority-based load shedding algorithm aimed at enhancing the stability of hybrid DC microgrids, maintaining power balance among various energy sources and storage devices during independent or prolonged islanding operation modes. Senapati et al.¹⁹ proposed a hybrid maximum power point tracking (MPPT) technique that combines an improved invasive weed optimization (MIWO) algorithm with the traditional perturb and observe (P&O) algorithm, enhancing the searching performance of PV systems under partial shading conditions (PSCs) and rapid climatic changes. Finally, they also proposed a hybrid firefly algorithm-particle swarm optimization (FA-PSO) approach, which combines the global search capability of the firefly algorithm with the rapid convergence of particle swarm optimization. This method can more effectively optimize the parameters of Takagi-Sugeno fuzzy inference systems (TSFIS) and adaptive neuro-fuzzy inference systems (ANFIS), thereby improving the voltage regulation performance and adaptability of DC microgrids²⁰.

Due to their ability to handle complex, high-dimensional, and nonlinear optimization problems, metaheuristic algorithms have recently been applied to the dynamic reconfiguration of distribution networks. For instance, an improved binary particle swarm optimization algorithm has been proposed to solve the low-power reconstruction model by effectively generating and updating particles to break loop constraints²¹. Additionally, a new hybrid optimization algorithm that combines chaotic particle swarm optimization and chicken swarm optimization has been proposed to overcome the limitations of traditional optimization algorithms in the reconfiguration of distribution networks²².

In recent years, more meta-heuristic algorithms have been developed successively, such as Harmonious Search algorithm (HS)²³, Grasshopper Optimization algorithm (GOA)²⁴, Gray Wolf Optimization algorithm (GWO)²⁵, Moth Flame Optimization algorithm (MFO)²⁶, Whale Optimization algorithm (WOA)²⁷, Dragonfly algorithm (DA)²⁸ and Dung Beetle algorithm (DBO)²⁹. Among them, DBO has a strong advantage in dealing with complex dynamic reconfiguration problems in distribution network. First of all, there are four different types of dung beetle individuals in DBO, each with different optimization methods, which gives the DBO a powerful global search ability, enabling it to effectively explore the solution space and quickly converge to the optimal reconstruction scheme. In addition, DBO is very suitable to deal with the nonlinear constraints that often occur in the distribution network reconstruction task, which ensures the accuracy of the reconstruction scheme. Its adaptive characteristics enable it to adapt to different load conditions in real time, thus maintaining the reliability of the system. These characteristics make DBO a powerful tool to realize efficient and reliable dynamic reconfiguration of distribution network. Although DBO has advantages such as global search capability and adaptability to dynamic conditions, there are also some challenges. Distribution network may also lead to multiple local optimal solutions under different reconfiguration schemes, which will hinder the ability of the algorithm to find the global optimal solution and limit its reliability in large-scale distribution networks.

Improvement methods for metaheuristic algorithms vary, leading to differences in the performance of the improved algorithms. To maximize the optimization ability and convergence of the algorithms while meeting the algorithm constraints, this study employs the Chebyshev chaotic mapping to enhance the population initialization stage of the DBO algorithm, enabling the individuals to be uniformly distributed randomly in the search space. Subsequently, the population is divided into four different types of beetles in a 6:6:7:11 ratio, and the Levy flight strategy is introduced into the population update mode to find the optimal position within the population and record the initial optimal values. In the subsequent phases of the procedure, the DE technique is introduced to choose, alter, and combine the initial optimal values, averting the algorithm from getting trapped in local minima. The resulting algorithm, named LDEDBO, is then applied to the dynamic reconstruction of the IEEE-33 and IEEE-69 node bus, obtaining the optimal switch combination solution with minimized network losses and minimal node voltage deviations.

The main findings of this paper are summarized as follows:

- A novel algorithm, LDEDBO, is introduced in this study.

- The proposed LDEDBO algorithm is applied to the optimal reconstruction of distribution network, and the feasibility of LDEDBO in the reconstruction of distribution network is verified by real-time load data.
- The proposed LDEDBO algorithm is applied to the dynamic reconfiguration of distribution network. Compared with PSO, GA and DBO algorithms, LDEDBO significantly increases the voltage of each node and reduces the active power loss of the system.

The organization of the remaining part of this document is outlined below: In “Issue definition”, the mathematical framework for distribution network reconstruction is introduced; In “Methodology”, an improved LDEDBO is presented. “Experimental design and results analysis” presents and scrutinizes the dynamic reconfiguration outcomes of the LDEDBO and the control group algorithm that have been validated. “Conclusion” gives a comprehensive conclusion.

Issue definition

Objective function

Active power dissipation

To enhance the economic efficiency of grid operation, the focus of this study is on pinpointing the most effective combination of network switches to minimize the active power dissipation within the grid^{6,30}. The formal representation of active power dissipation is as follows:

$$\min f_1 = P_{loss} = \sum_{t=1}^T \sum_{i=1}^N k_{i,t} R_{i,t} \frac{P_{i,t}^2 + Q_{i,t}^2}{V_{i,t}^2}. \quad (1)$$

where, P_{loss} is the cumulative active power dissipation of the whole network. T indicates a 24-h period. N indicates the overall count of system branches. The variable $k_{i,t}$ denotes the operating state of the switch on branch i at time t . Specifically, when $k_{i,t} = 1$, it indicates that the switch is in the closed position, while $k_{i,t} = 0$ denotes the switch being open. $R_{i,t}$ signifies the resistance along the i branch at time t . Additionally, $P_{i,t}$ and $Q_{i,t}$ are the active and reactive power flowing into the terminal node of branch i at time t , while $V_{i,t}$ signifies the voltage at the terminal node during time t .

Node voltage deviation

To fortify the stability of the power distribution system operation, this paper incorporates the minimization of node voltage deviation as one of its key objectives³¹. The formalized expression for node voltage deviation is presented below:

$$\min f_2 = \min \sum_{t=1}^T \sum_{i=1}^M \left| \frac{V_{i,t} - V_{iN,t}}{V_{iN,t}} \right| \quad (2)$$

where, M is the total number of nodes within the system, $V_{i,t}$ is the voltage amplitude of i at time t , and $V_{iN,t}$ signifies the rated voltage amplitude of i at time t .

Objective function normalization

When normalizing multi-objective functions, the method of judgment matrix is utilized to calculate the weight of each objective function³², with the total objective function designated as Eq. (3):

$$f = w_1 f_1 + w_2 f_2 \quad (3)$$

where, w_1 represents the weight of objective function f_1 , w_2 represents the weight of objective function f_2 . The expression equation of the judgment matrix is shown in Eqs. (4) and (5):

$$A = \begin{bmatrix} a_{11} & a_{12} & \cdots & a_{1n} \\ a_{21} & a_{22} & \cdots & a_{2n} \\ \vdots & \vdots & \ddots & \vdots \\ a_{n1} & a_{n2} & \cdots & a_{nn} \end{bmatrix} \quad (4)$$

$$a_{ij} = \frac{1}{a_{ji}} \quad (5)$$

where, n is the number of objective functions. a_{ij} is the comparison result of the importance of objective function i compared with objective function j . The specific value of a_{ij} needs to refer to the formation criteria of the judgment matrix. In this study, objective function f_1 is obviously more important than objective function f_2 , with values set as $a_{ij} = 5$, $a_{ji} = \frac{1}{5}$.

Sum each column of the judgment matrix to get the sum S_j , as Eq. (6):

$$S_j = \sum_{i=1}^n a_{ij} \quad (6)$$

The calculation formula of weight coefficient ω_j is shown as Eq. (7):

$$\omega_j = \frac{1}{n} \sum_{i=1}^n \frac{a_{ij}}{S_j} \quad (7)$$

The weight coefficients of the two objective functions obtained by the weight coefficient method are as follows: $w_1 = 83.33\%$, $w_2 = 16.67\%$.

Operational constraints

To prevent impractical outcomes that compromise the principles of safe and stable network operation, the refurbishment of the grid must comply with power transmission, nodal voltage, branch power, power generation, and network configuration constraints³³. Equation (8) illustrates the load flow restrictions.

$$\begin{cases} P_i + P_{DG_i} = P_{L_i} + V_i \sum_{j=1}^n V_j (G_{ij} \cos \theta_{ij} + B_{ij} \sin \theta_{ij}) \\ Q_i + Q_{DG_i} = Q_{L_i} + V_i \sum_{j=1}^n V_j (G_{ij} \sin \theta_{ij} - B_{ij} \cos \theta_{ij}) \end{cases} \quad (8)$$

where, P_i and Q_i denote the active power and reactive power of node i . The power injected by DG into node i is expressed in P_{DG_i} and Q_{DG_i} , and the power of the load attached to node i is expressed in P_{L_i} and Q_{L_i} . Node j is connected to i . The node voltages of nodes i and j are denoted by V_i and V_j , in that order. G_{ij} and B_{ij} represent the conductance and susceptance of nodes i and j , respectively. θ_{ij} is the angle of impedance between nodes i and j , and n is all count of nodes. Equation (9) is the constraints of node voltage:

$$V_{i,\min} \leq V_i \leq V_{i,\max} \quad (9)$$

where, $V_{i,\max}$ and $V_{i,\min}$ are the limits of node voltage V_i .

Equation (10) shows the constraints of branch power:

$$S_i \leq S_{i,\max} \quad (10)$$

where, $S_{i,\max}$ is the limits allowable power transmission capacity of branch i .

Equation (11) is the constraints of DG power:

$$\begin{cases} P_{DG,\min} \leq P_{DG,i} \leq P_{DG,\max} \\ Q_{DG,\min} \leq Q_{DG,i} \leq Q_{DG,\max} \end{cases} \quad (11)$$

where, $P_{DG,\max}$, $P_{DG,\min}$, $Q_{DG,\max}$ and $Q_{DG,\min}$ represents the limits of the DG's power generation, respectively.

Equation (12) is the constraint of network structure:

$$g \in G \quad (12)$$

where, g indicates the configuration of the power distribution system. G encompasses the entire set of network structures within the distribution system.

Methodology

DBO algorithm

The DBO algorithm is an intelligent optimization algorithm inspired by the motion process of rolling dung beetles²⁹. The population consists of four types of individuals: rolling beetles, female beetles, larvae beetles, and thief beetles, in the proportions of 6:6:7:11. Throughout the iterative procedure, the positional data of rolling beetles undergoes various updates, as defined by Eq. (13).

$$X_i(t+1) = X_i(t) + \alpha k X_i(t-1) + b |X_i(t) - X^W| \quad (13)$$

$$\lambda = 0.1, \eta = rand(1), \begin{cases} \eta > \lambda, \alpha = 1 \\ \eta < \lambda, \alpha = -1 \end{cases} \quad (14)$$

where, $i = 1, 2, 3, \dots, NP$; $X_i(t)$ represents the location of the i individual at the t step. The selection strategy for α depends on a constant λ and a random variable η . When $\alpha = 1$, it means that the dung beetle moves in the original direction, while $\alpha = -1$ represents the departure from the original goal. $k \in (0, 0.2]$ is the deviation parameter. $b \in (0, 1)$ is natural value too. X^W denotes the poorest position in the entire population.

When a rolling beetle hits a barrier, it updates its position as Eq. (15):

$$\begin{cases} X'_i(t) = \tan(\theta) |X_i(t) - X_i(t-1)| \\ X_i(t+1) = X_i(t) + X'_i(t) \end{cases} \quad (15)$$

Here, $\theta \in [0, \pi]$.

Female dung beetle spawning boundary and egg position update as follow:

$$Lb^* = \max \{X_i^* \times [1 - (1 - t/T_{max})], Lb\} \quad (16)$$

$$Ub^* = \min \{X_i^* \times [1 + (1 - t/T_{max})], Ub\} \quad (17)$$

$$\begin{cases} B_i^*(t) = b_1 (B_i(t) - Lb^*) + b_2 (B_i(t) - Ub^*) \\ B_i(t+1) = X_i^* + B_i^*(t) \end{cases} \quad (18)$$

where, Ub^* and Lb^* are the boundaries of the egg-laying area. X_i^* represents the current locally optimal position found during the search. T_{max} represents the maximum number of iterations. Ub and Lb are the boundaries of the optimization problem. $B_i(t)$ denotes the i -th sac position in the t step. b_1 and b_2 are two uncorrelated random vectors with a magnitude of $1 \times D$, where D represents the dimension of the distribution network reconfiguration problem.

The position of larvae in the population is simulated as Eq. (21):

$$Lb^b = \max \{X_i^b \times [1 - (1 - t/T_{max})], Lb\} \quad (19)$$

$$Ub^b = \min \{X_i^b \times [1 + (1 - t/T_{max})], Ub\} \quad (20)$$

$$\begin{cases} X_i^*(t) = C_1 (X_i(t) - Lb^b) + C_2 (X_i(t) - Ub^b) \\ X_i(t+1) = X_i(t) + X_i^*(t) \end{cases} \quad (21)$$

where, X^b is the global best location. Ub^b and Lb^b are the boundaries of the optimal foraging area. $X_i(t)$ is the location of the i larval beetle during the t iteration. C_1 represents a stochastic value following a normal distribution. C_1 is a random value within the range $(0, 1)$.

The equation for adjusting the location of the thief beetles, which emerge in the population to compete for food, is as Eq. (22):

$$X_i(t+1) = X_i^b(t) + \gamma\omega (|X_i(t) - X_i^*| + |X_i(t) - X_i^b(t)|) \quad (22)$$

where, setting $\gamma = 1/2$, while ω is defined as a vector of size $1 \times D$, with its variation pattern following a normal distribution during the algorithm iteration process. The final algorithm outputs $X_i^b(t)$ and the corresponding fitness value $f(X_i^b(t))$ according to greedy selection.

LDDEBO algorithm

To achieve a uniform distribution of the initial beetle population in the search space, the DBO utilizes Chebyshev chaotic mapping to improve the initialization, ensuring that individuals are uniformly distributed. Furthermore, the introduction of the Levy flight strategy equips beetle individuals with the ability to make long jumps, enabling them to explore the optimal solution in a wide space when updating their position information. Furthermore, to avert the algorithm from becoming ensnared in local optima during subsequent iterations, the DE is employed to modify the optimal solution of the DBO through a series of operations including mutation, crossover, and selection. This is referred to as the LDDEBO algorithm, and its implementation can further improve the overall performance and effectiveness of the algorithm.

Chebyshev chaotic mapping

The Chebyshev chaotic mapping is a nonlinear dynamical system that generates a series of numerical sequences with chaotic properties through recursive iteration. In the DBO algorithm, the Chebyshev chaotic mapping is introduced to initialize the dung beetle population, simulating the random search behavior of individual dung beetles, and increasing the variability and heterogeneity within the population. The position of the individual i is X_i :

$$X_{i+1} = \cos(h \cos^{-1} X_i), X_i \in [-1, 1] \quad (23)$$

In this context, h represents the order of the Chebyshev mapping. When the value of h is greater than 2, it generates an infinite-length chaotic sequence without a periodic pattern. It is common to set $h = 4$ in practice.

Levy flight strategy

The long-tail distribution of Levy flight steps makes it possible to have large jumps in the search space. This method is introduced into the DBO algorithm to improve the location modification mode of beetles and help to escape from the local optimum. The particular equation is outlined below:

$$\begin{cases} X_i(t+1) = X_i(t) + S \\ S = 0.01 * Step = 0.01 * \frac{a}{|b|^{1/c}} \\ a \sim randn(1, D) * e, b \sim randn(1, D) \end{cases} \quad (24)$$

$$e = \left\{ \frac{T(1+c) \sin(\pi c/2)}{T \left[\frac{(1+c)c}{2} \right] c^{2(c-1)/2}} \right\}^{1/c} \quad (25)$$

The function first defines the parameter c of the Levy distribution as 1.5 and calculates e according to the formula. Subsequently, the *randn* function is utilized to generate standard normal distribution random numbers a and b with a dimension of $D = 5$. The step length *Step* is then calculated based on the Levy flight formula and multiplied by 0.01 to obtain the final step vector S .

DE algorithm

DE approach is a parallel direct search technique employed to handle non-differentiable, complex and multi-peaked objective functions³⁴. After the DBO algorithm obtains the initial optimal solution $X_i^b(t)$, two individuals are randomly selected and the weighted difference between them is controlled by the scale factor. The resulting vector is added to $X_i^b(t)$ to create a new individual, completing the mutation process. Then, $X_i^b(t)$ is crossed with its autogenetic offspring with a certain probability to increase the diversity of perturbation parameter vectors. When the resulting individual's fitness is lower than $f(X_i^b(t))$, the target candidate is replaced and the next iteration is continued until the maximum number of iterations is reached. To improve the optimization performance of the algorithm, this study proposed to combine the DE with the DBO. Using this approach, two independent positions $X_{i1}(t)$ and $X_{i2}(t)$ are randomly chosen from the set, and an individual is created after mutation, as illustrated in Eq. (26):

$$V_i(t) = X_i^b(t) + F * (X_{i1}(t) - X_{i2}(t)) \quad (26)$$

where, $F \in [0, 2]$ is the variation factor. The intersection of $V_i(t)$ and the initial optimal entity $X_i^b(t)$, which was generated by the DBO algorithm, gives rise to a novel vector entity, $U_{i,j}(t)$:

$$U_{i,j}(t) = \begin{cases} V_{i,j}(t), & \text{if } \text{ifrand}(0, 1) \leq CR \text{ or } j = jrand \\ X_{i,j}^b(t), & \text{otherwise} \end{cases} \quad (27)$$

where, $j = 1, 2, 3, \dots, D$. $CR \in (0, 1)$ is a cross probability factor; $jrand$ is a random component.

Following the selection operation, $X_i^b(t+1)$ becomes a newly global optimal solution:

$$X_i^b(t+1) = \begin{cases} U_i(t), & \text{if } f(U_i(t)) \leq f(X_i^b(t)) \\ X_i^b(t), & \text{otherwise} \end{cases} \quad (28)$$

The algorithm diagram for LDEDDBO can be seen in Fig. 1.

Algorithm testing

This study selects 9 common test functions to evaluate LDEDDBO's algorithm performance. The test results of GA, PSO, WOA, HHO, and DBO as control algorithms are compared with those of the LDEDDBO algorithm. We set key performance indicators such as best value (BEST), average value (MEAN), standard deviation (STD), and algorithm runtime (TIME) to evaluate its convergence accuracy, stability, robustness, and time complexity.

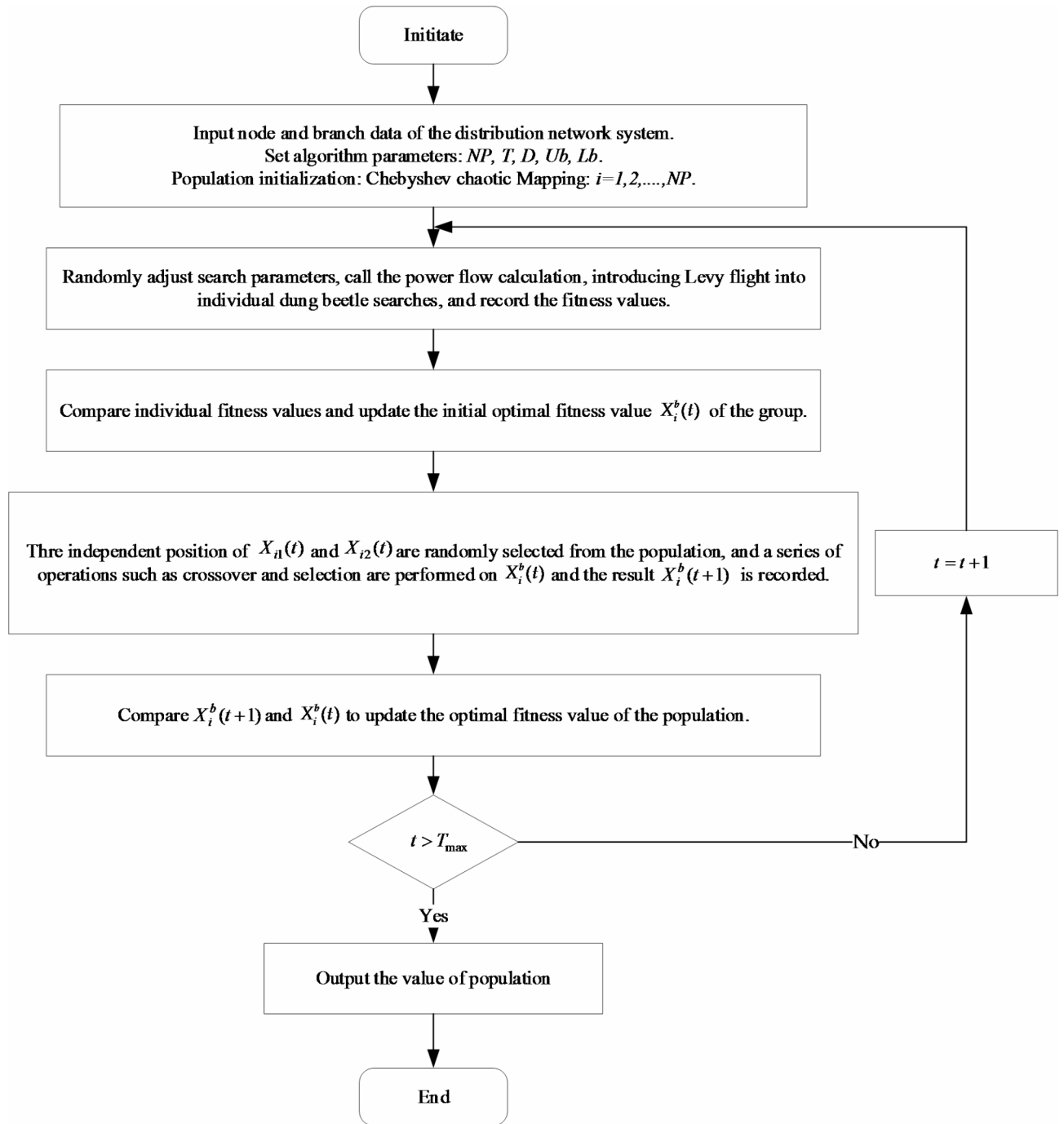


Fig. 1. Flowchart of LDEDBO algorithm.

Algorithm parameters are set as shown in Table 1. The formulas and parameters of relevant test functions are shown in Table 2. Each algorithm is initialized with a total initial population size of 30, runs 30 times, and iterates 600 times each. The test results are shown in Table 3, and the convergence curve of each algorithm is shown in Fig. 2.

According to the test results, the optimal value of LDEDBO algorithm is obviously better than that of the control algorithm, which indicates that LDEDBO algorithm has good optimization ability. The average index is close to the optimal value, reflecting the average result of LDEDBO's overall performance in many runs, which indicates that it has good stability. And the standard deviation index is small, indicating that LDEDBO algorithm has good robustness. Although the LDEDBO algorithm is slightly worse than the control group in terms of runtime, the gap is not significant, and considering its advantages in other performance indicators, LDEDBO algorithm still shows a strong overall performance. The slight increase in the running time of LDEDBO algorithm may be due to the complexity of the calculation process caused by the addition of an improved strategy on the

Algorithms	Parameters
GA	$pm = 0.05, pc = 0.8$
PSO	$C_{1,2} = 1.43, \omega \in [0.4, 0.9]$
WOA	$\alpha \in (0, 2)$
HHO	$E_0 \in (-1, 1)$
DBO	$k = 0.1, b = 0.3, \gamma = 1/2$
LDEDDBO	$k = 0.1, b = 0.3, \gamma = 1/2, h = 4, F = 0.8, CR = 0.9, \lambda = 0.1$

Table 1. GA, PSO, DBO and LDEDDBO parameter configurations.

Function	Dim	Min
$F_1(x) = \sum_{i=1}^n x_i^2$	30	0
$F_2(x) = \sum_{i=1}^n x_i + \prod_{i=1}^n x_i $	30	0
$F_3(x) = \sum_{i=1}^n (\sum_{j=1}^i x_j)^2$	30	0
$F_4(x) = \max\{ x_i , 1 \leq i \leq n\}$	30	0
$F_5(x) = -20 \exp(-0.2 \sqrt{\frac{1}{n} \sum_{i=1}^n x_i^2}) - \exp(\frac{1}{n} \sum_{i=1}^n \cos(2\pi x_i)) + 20 + e$	30	0
$F_6(x) = \frac{\pi}{n} \{10 \sin(\pi y_1) + \sum_{i=1}^{n-1} (y_i - 1)^2 [1 + 10 \sin^2(\pi y_{i+1})] + (y_n - 1)^2\} + \sum_{i=1}^n u(x_i, 10, 100, 4),$ $y_i = 1 + \frac{x_i + 1}{4}$	30	0
$F_7(x) = \sum_{i=1}^{11} [a_i - \frac{x_1(b_i^2 + b_i x_2)}{b_i^2 + b_i x_3 + x_4}]^2$	4	0.0003075
$F_8(x) = -\sum_{i=1}^4 c_i \exp(-\sum_{j=1}^6 a_{ij} (x_j - p_{ij})^2)$	6	-3.32
$F_9(x) = -\sum_{i=1}^5 [(x - a_i)(x - a_i)^T + c_i]^{-1}$	4	-10

Table 2. Test function settings.

basis of the original DBO algorithm, but it also provides LDEDDBO with higher accuracy and better robustness. Therefore, in summary, LDEDDBO algorithm shows excellent performance in the test results, especially in solving complex problems, which is worthy of further promotion and application.

Experimental design and results analysis

When reconfiguring dispersed electricity distribution networks, the fluctuating nature of actual load demand necessitates a shift from static reconfiguration at a single time point to dynamic reconfiguration. In this study, we address this by reconfiguring the time-varying load into five distinct periods based on the rising and falling trends observed in the load power curve depicted in Fig. 3. Subsequent simulation experiments were conducted using the MATLAB platform. Throughout all experimental scenarios, control group experiments were conducted using DBO, PSO, and GA algorithms, with specific parameter settings detailed in Table 1. Each algorithm underwent independent runs 30 times, with varying numbers of iterations designed according to the experimental plan. Key metrics including average active network losses, minimum nodal voltage, and the switch configuration linked to the minimum performance value were recorded for analysis.

Simulation and analysis of case 1: IEEE-33 node bus

In the structure of the IEEE-33 node bus, there are 32 feeders, 33 connection points, 32 isolating switches, 5 interconnection switches, and 5 primary loops. The initial base capacity of the network is 10 MVA, with a standard load of 3715 kW + j2300 kVar, and a reference voltage of 12.66 kV. In the experiment, wind energy sources are used as PQ-type nodes, photovoltaic sources as PI-type nodes, and gas turbines are linked to the distribution network as PV-type components, with the installation positions of DG shown in Fig. 4. Table 4 provides the specific parameters of the DG. Real-time load data at 05:00, 10:00, and 20:00 are randomly selected from the daily load curve for the purpose of reconfiguration. Each algorithm is set to undergo 50 iterations.

The experimental results presented in Table 5 clearly demonstrate the superior performance of LDEDDBO over other control methods for optimizing the two objective functions, namely minimum active power

Functions	Index	GA	PSO	WOA	HHO	DBO	LDEDDBO
F ₁	BEST	10499.1679	0.0002756	3.53E-101	7.04E-133	1.78E-204	8.07E-302
	MEAN	19498.0397	0.015439	5.98E-89	1.42E-115	1.69E-134	5.82E-214
	STD	7150.4176	0.02492	3.26E-88	5.02E-115	8.91E-134	0
	TIME	0.075835	0.055012	0.046318	0.09976	0.10209	0.1048
F ₂	BEST	33.6167	0.065757	4.10E-67	3.64E-74	2.19E-100	1.26E-138
	MEAN	53.6898	1.6907	5.97E-59	3.26E-60	5.63E-65	4.46E-114
	STD	11.5429	1.5793	3.26E-58	1.45E-59	3.08E-64	2.44E-113
	TIME	0.078982	0.058725	0.049809	0.10234	0.11028	0.11333
F ₃	BEST	32900.2626	52.4841	13943.721	2.27E-115	1.84E-164	4.88E-257
	MEAN	55324.6567	369.984	35695.095	8.21E-92	2.87E-85	4.93E-99
	STD	16505.4311	247.9008	9007.6008	3.09E-91	1.57E-84	2.70E-98
	TIME	0.24504	0.22134	0.2136	0.51225	0.27849	0.27978
F ₄	BEST	45.353	1.4891	4.196	3.77E-65	4.64E-98	2.27E-129
	MEAN	70.5708	3.2491	57.158	3.31E-58	3.60E-66	8.92E-105
	STD	11.2342	0.94879	26.5668	1.79E-57	1.95E-65	4.88E-104
	TIME	0.079827	0.060015	0.048497	0.13013	0.1093	0.11103
F ₅	BEST	19.3088	1.3514	4.44E-16	3.95E-14	0.00058442	4.44E-16
	MEAN	20.0295	2.1246	2.58E-15	4.20E-14	0.0008647	4.44E-16
	STD	0.33065	0.62958	2.48E-15	3.76E-15	0.00029371	0
	TIME	0.10421	0.075533	0.062343	0.14602	0.37277	0.12631
F ₆	BEST	218.4346	0.0008395	0.0023575	0.01312	3.82E-07	2.43E-08
	MEAN	8156864.642	1.094	0.016944	0.03715	1.19E-06	0.00011169
	STD	13960298.39	1.0965	0.022174	0.014297	7.00E-07	0.00029825
	TIME	0.37941	0.34449	0.34241	0.42971	0.69909	0.41919
F ₇	BEST	0.0009885	0.0003075	0.0003095	0.00030749	0.0003136	0.00030749
	MEAN	0.010339	0.0008148	0.001156	0.0050124	0.0027021	0.0008233
	STD	0.008073	0.0003494	0.0020847	0.0086136	0.0059902	0.00038043
	TIME	0.076245	0.026711	0.039919	0.047216	0.052875	0.096752
F ₈	BEST	-2.9317	-3.322	-3.3218	-3.322	-3.322	-3.322
	MEAN	-1.692	-3.2744	-3.2152	-3.2776	-3.2201	-3.2348
	STD	0.57755	0.059241	0.12122	0.072339	0.052668	0.092416
	TIME	0.095941	0.040054	0.055393	0.069391	0.071979	0.11859
F ₉	BEST	-1.9565	-10.1532	-10.1531	-10.0781	-10.1532	-10.1532
	MEAN	-0.95066	-6.1035	-8.8556	-5.5473	-7.7833	-7.619
	STD	0.48134	3.1181	2.3653	1.5112	2.5736	2.5768
	TIME	0.10913	0.046623	0.06135	0.18155	0.12547	0.12346

Table 3. Algorithm test results.

dissipation and voltage fluctuation. The discovery strongly supports the potential use of LDEDDBO for addressing the reconstruction challenge in minor distribution grids. Figure 5 illustrates the voltage restoration outcomes at three randomly selected moments, revealing a smoother overall contour of the voltage curve reconstructed by the LDEDDBO compared to other algorithms. Furthermore, Fig. 6 showcases the convergence behavior of the different algorithms during the reconstruction process at these three moments. At 05:00, the LDEDDBO exhibits a slightly slower convergence speed than the PSO algorithm. However, when considering the convergence curves across all three moments, the PSO algorithm demonstrates unstable convergence speed and fails to effectively find the optimal solution. In contrast, the LDEDDBO consistently achieves convergence within 15 iterations, highlighting its exceptional accuracy and stability.

Following that, this article investigates the dynamic reconfiguration problem of small-scale distribution networks and designs the reconfiguration period according to the trend of daily load curve. The number of iterations for each algorithm is fixed at 200. The convergence plots of different algorithms are compared in Fig. 7. The LDEDDBO achieves a superior switching combination solution compared to other algorithms at the 28th step.

Table 6 presents the experimental data recorded under this set of switching combinations. The results indicate a significant decrease in active power dissipation from 1950.4 kW to 1385.9 kW, representing a decrease of 28.94%. In comparison, the reductions achieved by GA, PSO, and DBO algorithms are 19.82%, 15.79%, and 20.53% respectively. Additionally, the minimum node voltage stands at 0.9447 p.u., surpassing the previous value of 0.9273 p.u. Figure 8 illustrates the active power loss curves under different reconstruction algorithms. It clearly shows that after the LDEDDBO reconstruction, the active power dissipation at each node in the IEEE33

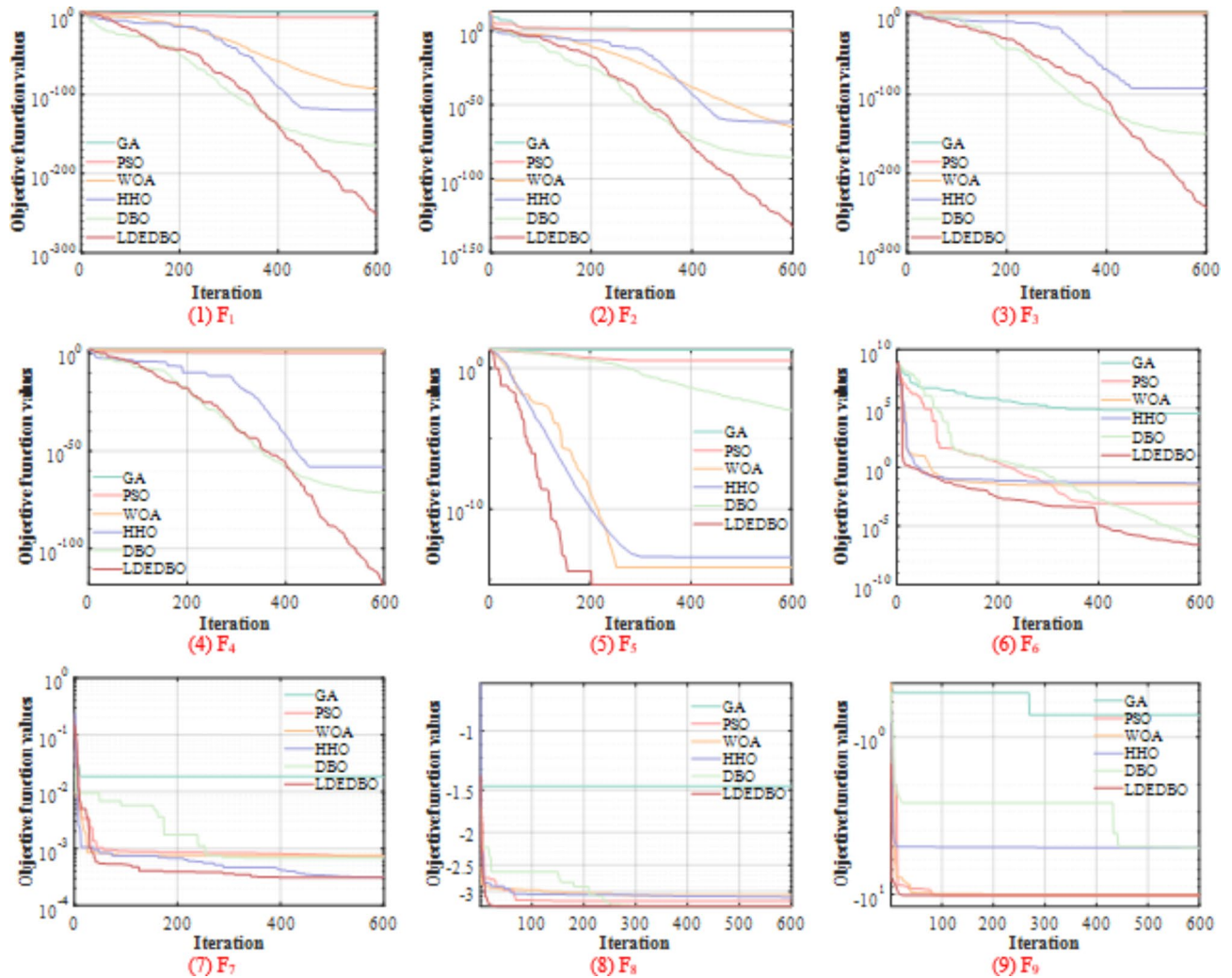


Fig. 2. Algorithm test curve.

node bus is less than 20 kW per hour. Figure 9 compares the overall voltage curves under various reconstruction algorithms. It shows that after the LDEDDBO reconstruction, the node voltages fluctuate more smoothly over 24 h. This indicates the stability and optimization ability of the LDEDDBO.

Simulation and analysis of case 2: IEEE-69 node bus

The structure of the IEEE-69 bus medium-scale power grid includes 73 branches, 69 nodes, and 68 isolating switches, 5 interconnection switches, and 5 primary loops. The initial reference capacity of the network is 10 MVA, with a standard load of 3802 kW + j2694.6 kVar, and a reference voltage of 12.66 kV. In the experiment, the installation positions of wind energy sources, photovoltaic sources, and gas turbines are shown in Fig. 10, with specific parameters detailed in Table 7. Real-time load data at 05:00, 10:00, and 17:00 are randomly selected from the daily load curve for reconstruction. Each algorithm is set to undergo 100 iterations.

The reconstruction results are presented in Table 8, further validating the feasibility of the LDEDDBO in the reconstruction of medium-scale distribution networks. In Fig. 11, the overall voltage profile after reconstruction using the LDEDDBO appears smoother compared to other algorithms, meeting the stability requirements of the power grid operation. In Fig. 12, the LDEDDBO converges to the optimal value within 10 iterations in all three scenarios, demonstrating the exceptional optimization performance and rapid convergence of the LDEDDBO in addressing medium-scale distribution network reconstruction problems.

After confirming the effectiveness of the LDEDDBO in the reconstruction challenge of medium-scale power grids, the LDEDDBO was utilized for the dynamic reconstruction of the IEEE-69 medium-scale node bus. All algorithm parameters remained constant, with the iteration count fixed at 200. Figure 13 presents a comparison of the convergence patterns of the various algorithms. The LDEDDBO achieved the optimal solution at the 32nd iteration.

Table 9 records the reconstruction results of each algorithm under the optimal network switch combination. The power dissipation after reconstruction by the LDEDDBO decreased from 2498.7 kW before reconstruction to 1588.0 kW, a reduction of 36.45%, which is significantly higher than the reductions achieved by the GA,

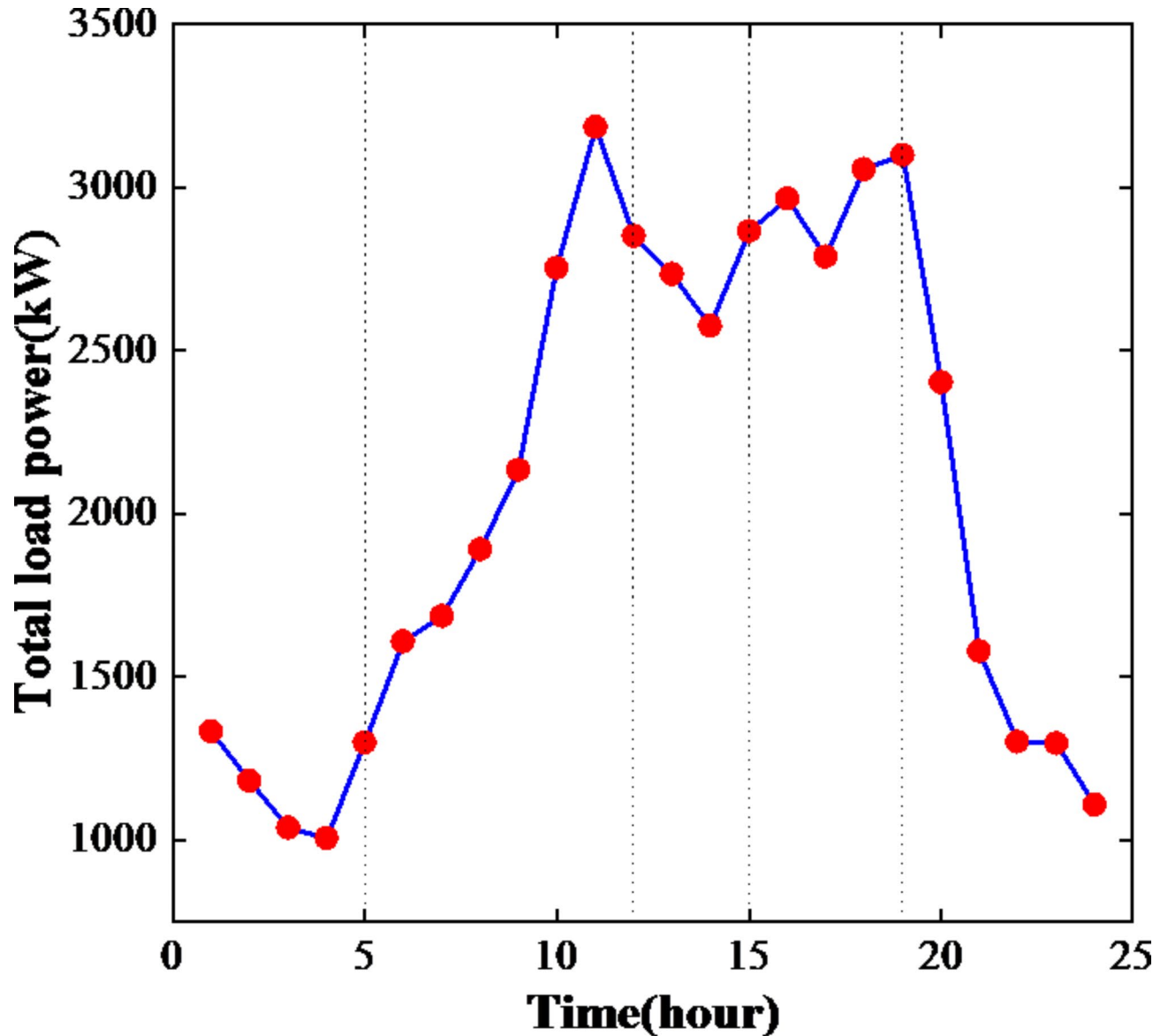


Fig. 3. Aggregate power consumption fluctuation curve of the network throughout a 24-h timeframe.

PSO, and DBO algorithms, which were 30.52%, 24.00%, and 33.43%, respectively. Figure 14 shows the power dissipation curves under the reconstruction of each algorithm, and after reconstruction by the LDEDDBO, the power dissipation curve of each time period in the IEEE-69 node bus is notably reduced compared to the other algorithms. Following the reconstruction by the LDEDDBO algorithm, the minimum node voltage increased from 0.9224 p.u to 0.9481 p.u, as shown in Fig. 15, which presents the overall voltage curves under the reconstruction of each algorithm. The voltage profiles of individual nodes after reconstruction through the LDEDDBO approach the standard value of 1 within 24 h. This outcome substantiates the effectiveness of the introduced LDEDDBO approach in tackling the dynamic reconstruction challenge of medium-scale distribution networks under time-varying loads.

Conclusion

The present study proposes a dynamic reconfiguration model for distribution networks that integrates an improved meta-heuristic algorithm. First, the DBO algorithm is enhanced using Chebyshev chaotic mapping, Levy flight, and differential evolution algorithms to develop the intelligent algorithm LDEDDBO. Next, the feasibility of the LDEDDBO algorithm in addressing the reconfiguration problem of distribution networks is validated under specific equivalent load conditions. Finally, for distribution networks with load fluctuations, reconfiguration time periods are determined based on the load curve trends, and the LDEDDBO algorithm is employed to obtain the optimal reconfiguration schemes for each time period, ensuring minimal active power losses and minimal voltage deviations.

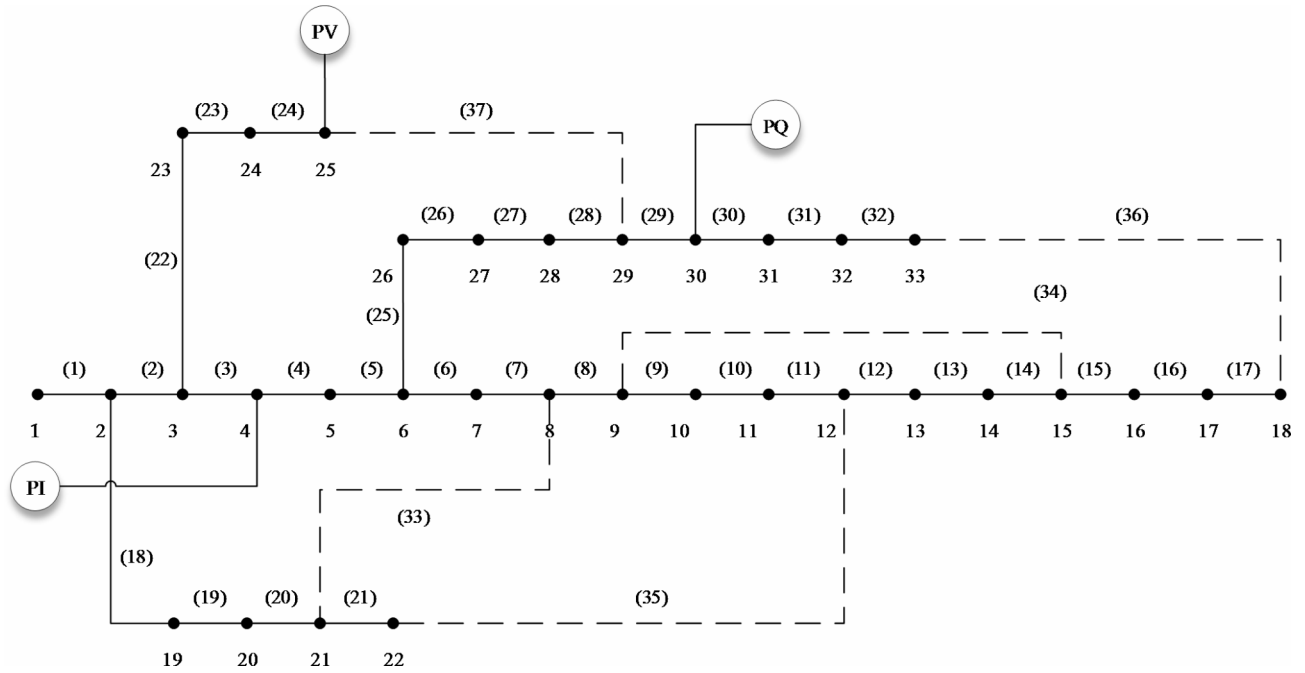


Fig. 4. Installation position of the DG in the IEEE-33 small-scale node bus.

DG type	Node	Parameters
PI	4	$P = 300 \text{ kW}, I_S = 50 \text{ A}$
PV	25	$P = 200 \text{ kW}, V_S = 0.98 \text{ p.u.}$
PQ	30	$P = 300 \text{ kW}, \cos \varphi = 0.9$

Table 4. The characteristics of various DG categories in the IEEE-33 small-scale node bus.

Method	Moments	Power dissipation (kW)	Minimum node voltage (p.u)	Open switches
Before	05:00	255.5795	0.9408	33, 34, 35, 36, 37
	10:00	481.5029	0.8621	33, 34, 35, 36, 37
	20:00	573.9049	0.8385	33, 34, 35, 36, 37
GA	05:00	139.2407	0.9705	33, 13, 9, 32, 28
	10:00	259.6344	0.9141	33, 14, 9, 32, 28
	20:00	338.8216	0.8979	33, 9, 7, 36, 28
PSO	05:00	136.6211	0.9686	33, 14, 9, 32, 28
	10:00	275.378	0.9071	33, 34, 11, 32, 28
	20:00	332.3553	0.9040	33, 14, 9, 32, 28
DBO	05:00	146.6389	0.9470	33, 34, 11, 36, 28
	10:00	250.1139	0.9142	33, 14, 9, 32, 28
	20:00	378.2845	0.8943	7, 9, 35, 36, 28
LDEDDBO	05:00	134.7648	0.9686	33, 14, 9, 32, 28
	10:00	247.8874	0.9152	7, 14, 10, 32, 28
	20:00	318.453	0.9040	7, 14, 9, 32, 28

Table 5. GA, PSO, DBO and LDEDDBO algorithms time reconstruction results of IEEE-33 small-scale node bus.

The experimental results are as follows: in the IEEE-33 small node bus, network active power losses are reduced by 28.94%, while the node voltage increases from 0.9273 p.u to 0.9447 p.u; in the IEEE-69 medium node bus, network active power losses are reduced by 36.45%, with the node voltage rising from 0.9224 p.u to 0.9481 p.u.

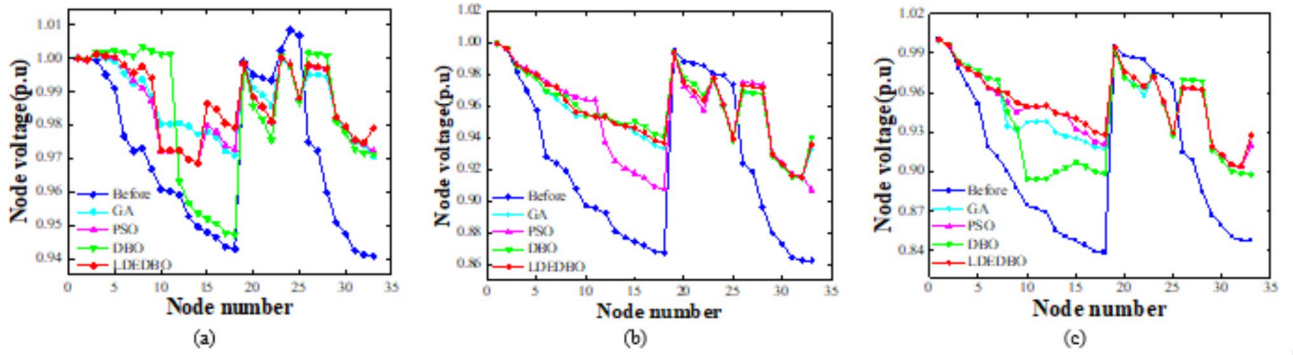


Fig. 5. Node voltage distribution in case 1: (a) At 05:00; (b) At 10:00; (c) At 20:00.

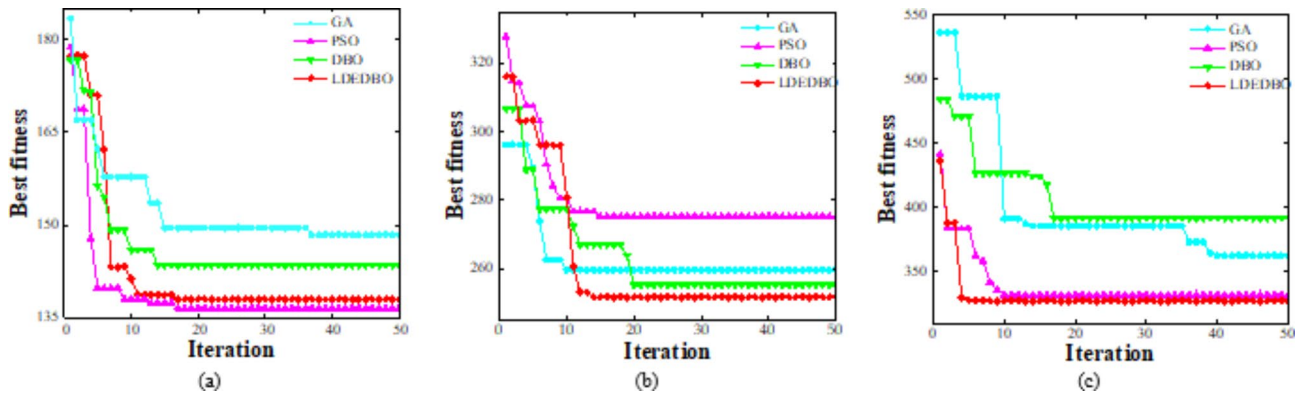


Fig. 6. Convergence curve in case 1: (a) At 05:00; (b) At 10:00; (c) At 20:00.

Based on the established model, future research needs to delve deeper into the following aspects: (1) Considering the impact of time-varying DG on the dynamic reconfiguration model of distribution networks based on time-varying loads; (2) Exploring more reasonable methods for dividing reconfiguration time periods; (3) Reducing the time complexity of the algorithm while enhancing its convergence accuracy, stability, and robustness.

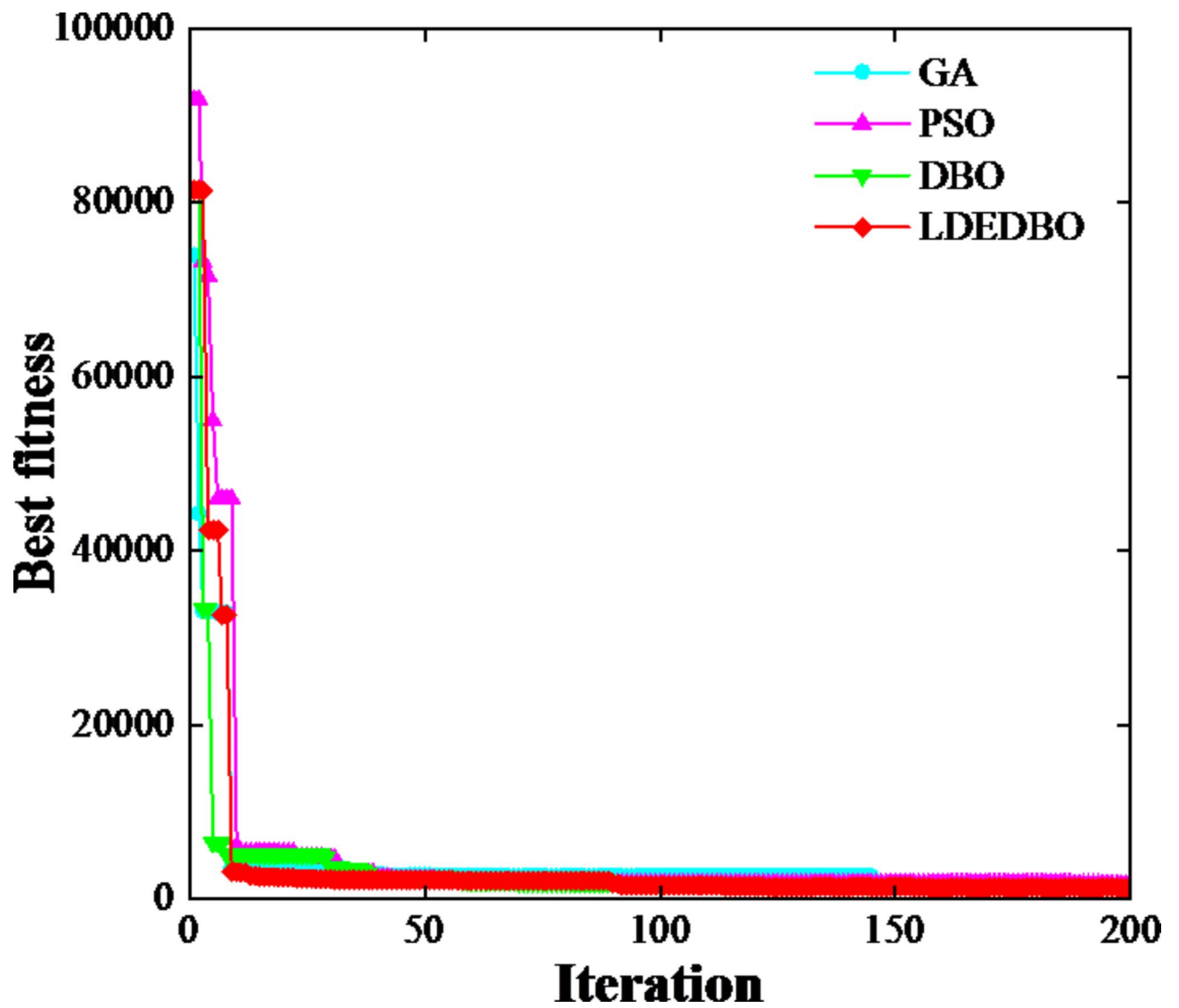


Fig. 7. The convergence curve for LDEDDBO in comparison to alternative algorithms.

Method	Power Dissipation(kW)	Minimum node voltage (p.u)	Time period	Open switches
Before	1950.4	0.9273	Total period	33, 34, 35, 36, 37
GA	1563.9	0.9416	00:00–04:00	6, 12, 10, 16, 28
			05:00–11:00	6, 14, 8, 16, 26
			12:00–14:00	3, 13, 10, 16, 28
			15:00–19:00	6, 13, 11, 15, 26
			20:00–24:00	7, 13, 11, 16, 27
PSO	1684.5	0.9311	00:00–04:00	18, 12, 11, 29, 28
			05:00–11:00	20, 13, 10, 15, 28
			12:00–14:00	33, 13, 10, 30, 37
			15:00–19:00	33, 13, 11, 31, 28
			20:00–24:00	33, 13, 10, 31, 28
DBO	1550.0	0.9439	00:00–04:00	7, 34, 9, 29, 25
			05:00–11:00	7, 13, 11, 31, 37
			12:00–14:00	7, 13, 10, 32, 26
			15:00–19:00	7, 34, 10, 36, 28
			20:00–24:00	33, 14, 7, 32, 37
LDEDBO	1385.9	0.9447	00:00–04:00	7, 13, 8, 16, 22
			05:00–11:00	7, 13, 9, 16, 37
			12:00–14:00	7, 14, 9, 16, 37
			15:00–19:00	7, 12, 35, 16, 37
			20:00–24:00	7, 14, 11, 16, 37

Table 6. GA, PSO, DBO and LDEDBO multi-period dynamic reconfiguration analyses of IEEE-33 small-scale node bus.

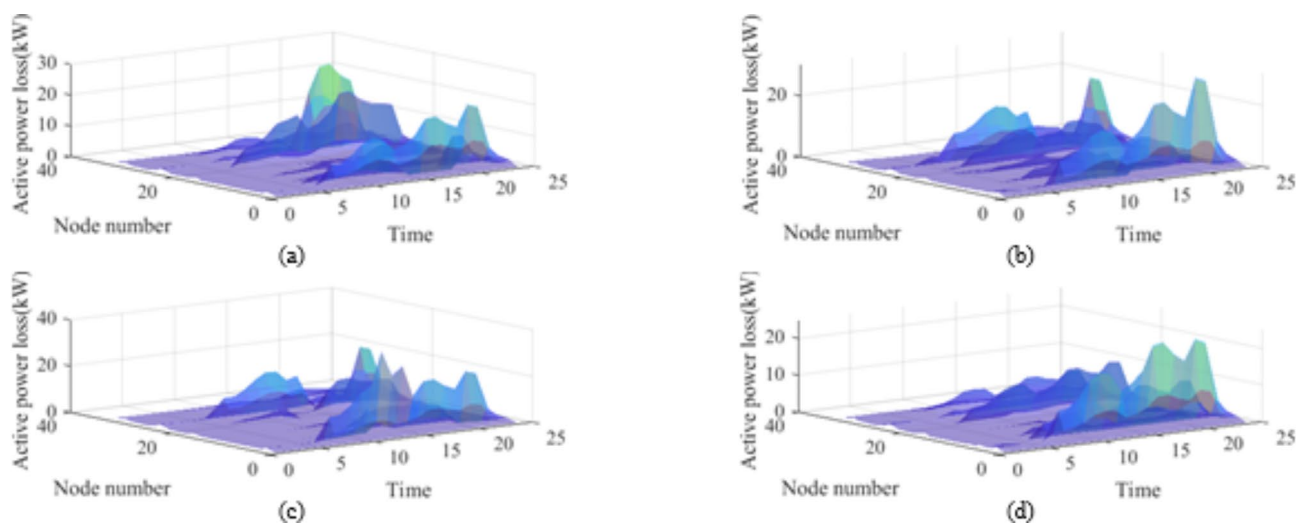


Fig. 8. Active power dissipation of IEEE-33 small-scale node bus in 24 h: (a) GA; (b) PSO; (c) DBO; (d) LDEDBO.

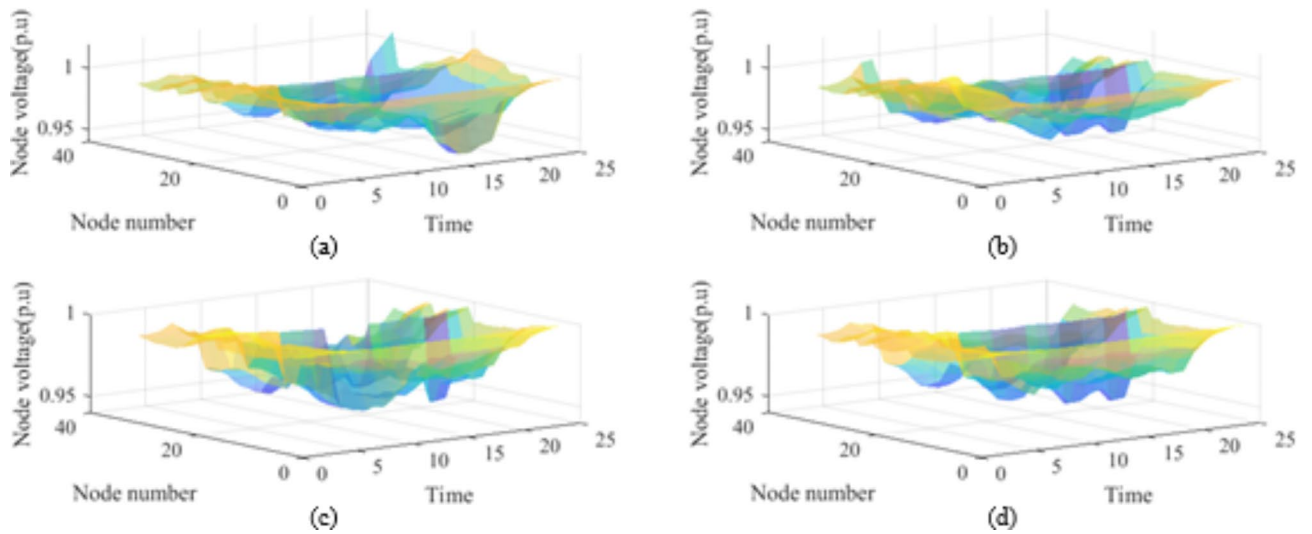


Fig. 9. Voltage fluctuation of IEEE-33 small-scale node bus in 24 h: (a) GA; (b) PSO; (c) DBO; (d) LDEDBO.

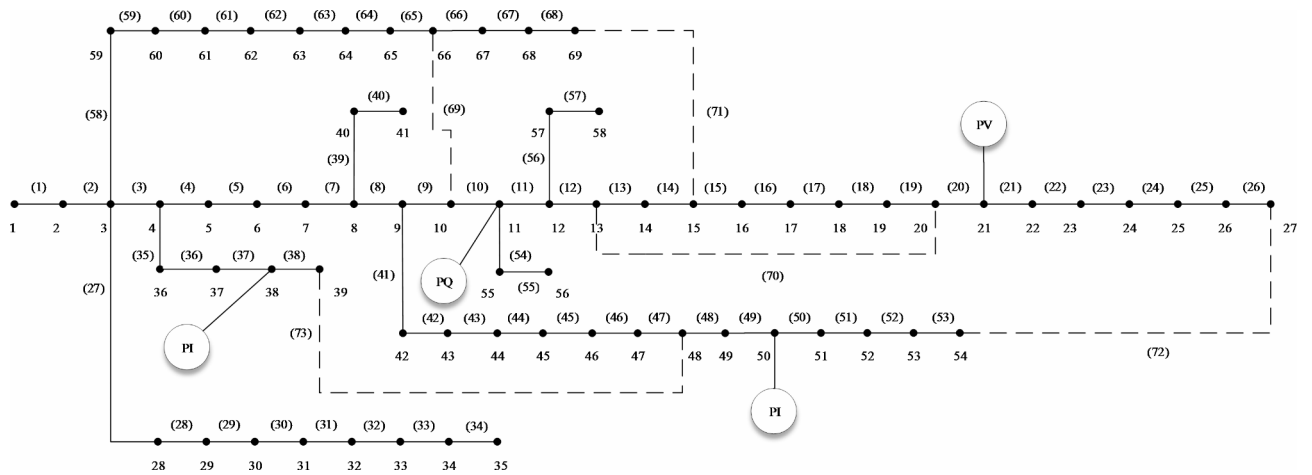


Fig. 10. Installation position of the DG in the IEEE-69 medium-scale node bus.

DGs type	Node	Parameters
PQ	11	$P = 300 \text{ kW}, \cos \varphi = 0.9$
PV	21	$P = 200 \text{ kW}, V_S = 0.98 \text{ p.u.}$
PI	38	$P = 300 \text{ kW}, I_S = 50 \text{ A}$
PI	50	$P = 300 \text{ kW}, I_S = 50 \text{ A}$

Table 7. The characteristics of various DG categories in the IEEE-69 medium-scale node bus.

Method	Moments	Power dissipation (kW)	Minimum Node voltage (p.u)	Open switches
Before	05:00	247.8767	0.9074	69, 70, 71, 72, 73
	10:00	654.0593	0.8569	69, 70, 71, 72, 73
	17:00	832.9785	0.8403	69, 70, 71, 72, 73
GA	05:00	125.4677	0.9313	10, 70, 71, 25, 47
	10:00	301.4934	0.9110	10, 70, 71, 72, 47
	17:00	373.1925	0.9051	69, 70, 12, 72, 47
PSO	05:00	122.0973	0.9313	69, 70, 12, 25, 47
	10:00	328.6242	0.9110	69, 70, 71, 72, 47
	17:00	373.4850	0.9251	69, 70, 11, 72, 47
DBO	05:00	120.5803	0.9297	10, 14, 11, 72, 47
	10:00	295.5287	0.9110	10, 70, 12, 72, 47
	17:00	343.5375	0.9052	100, 14, 11, 72, 47
LDEDDBO	05:00	101.3712	0.9394	69, 14, 11, 50, 47
	10:00	236.5193	0.9293	10, 13, 11, 50, 47
	17:00	307.4457	0.9052	69, 13, 11, 50, 47

Table 8. GA, PSO, DBO and LDEDDBO algorithms time reconstruction results of IEEE-69 medium-scale node bus.

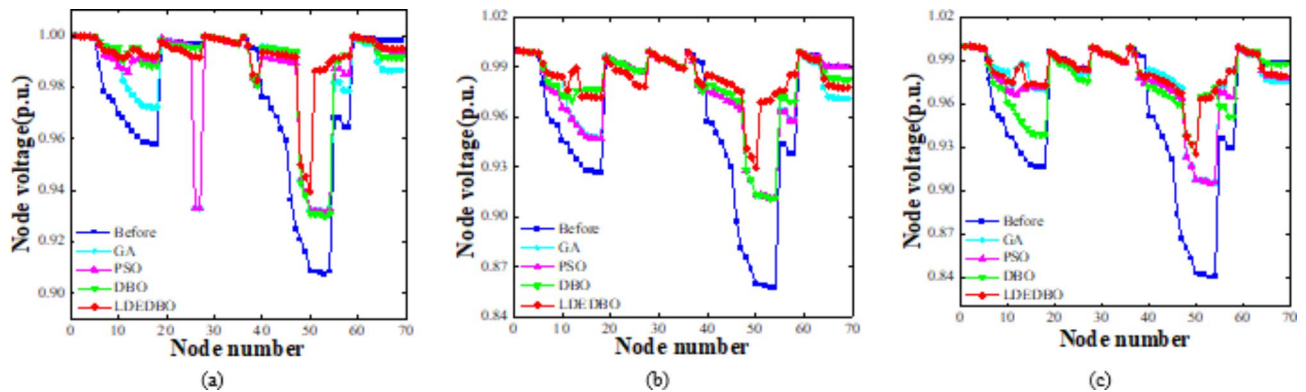


Fig. 11. Node voltage distribution in case 2: (a) At 05:00; (b) At 10:00; (c) At 17:00.

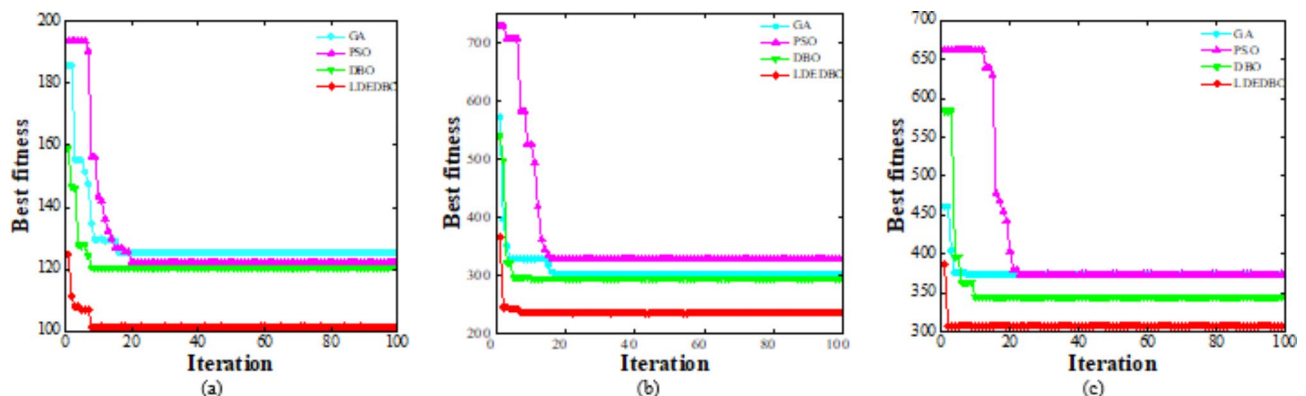


Fig. 12. Convergence curve in case 2: (a) At 05:00; (b) At 10:00; (c) At 17:00.

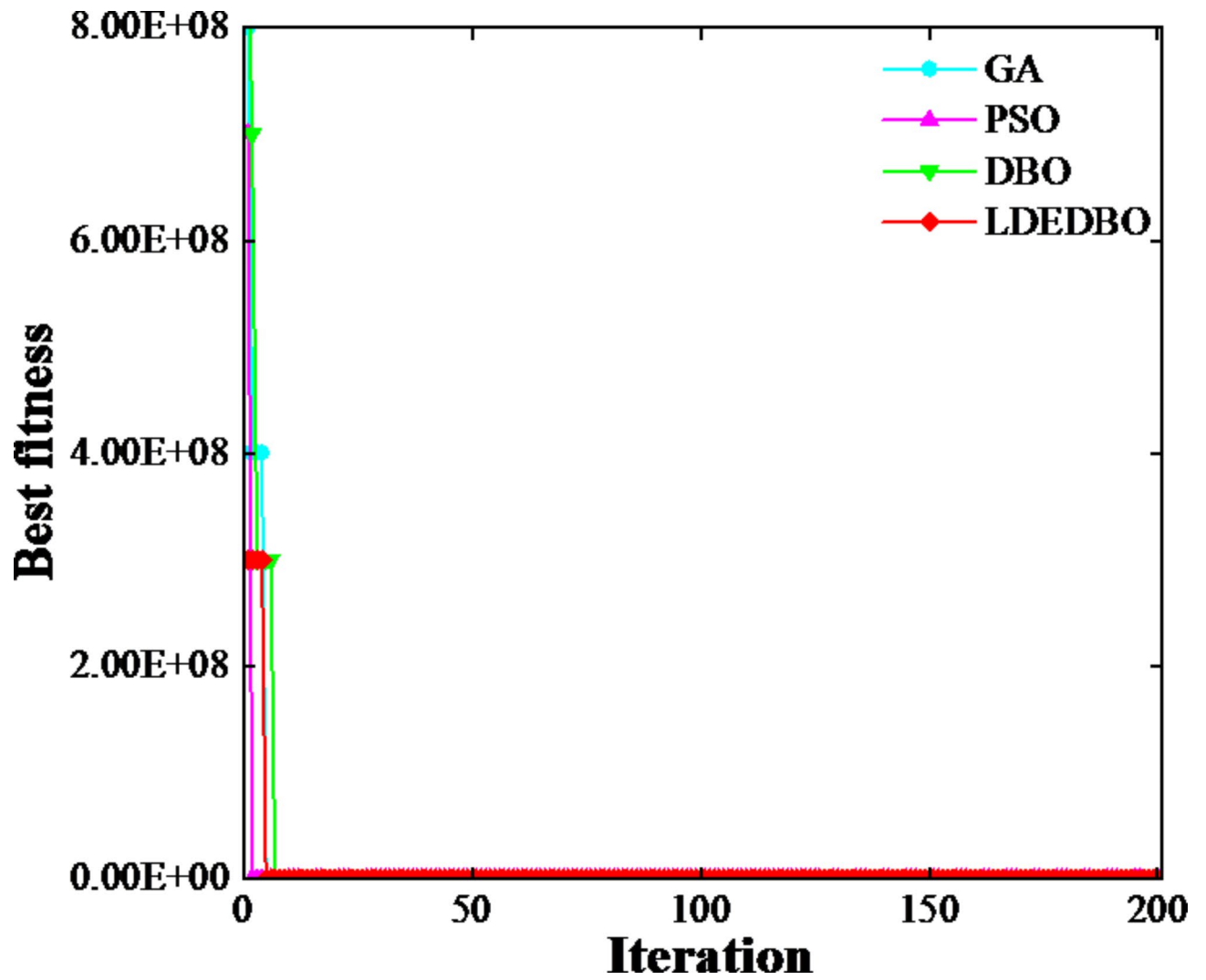


Fig. 13. Comparison of convergence curve of LDEDDBO with other algorithms.

Method	Power dissipation (kW)	Minimum node voltage (p.u)	Time period	Open switches
Before	2498.7	0.9224	Total period	69, 70, 71, 72, 73
GA	1736.0	0.9213	00:00–04:00	69, 70, 71, 53, 73
			05:00–11:00	10, 70, 14, 53, 73
			12:00–14:00	69, 13, 11, 72, 47
			15:00–19:00	69, 70, 71, 72, 47
			20:00–24:00	69, 70, 71, 72, 38
PSO	1899.1	0.9224	00:00–04:00	69, 70, 71, 47, 38
			05:00–11:00	69, 70, 12, 72, 73
			12:00–14:00	69, 70, 14, 53, 73
			15:00–19:00	69, 70, 12, 72, 38
			20:00–24:00	69, 70, 71, 72, 46
DBO	1663.5	0.9465	00:00–04:00	69, 70, 68, 26, 47
			05:00–11:00	65, 70, 71, 26, 45
			12:00–14:00	65, 70, 68, 26, 47
			15:00–19:00	69, 70, 13, 25, 47
			20:00–24:00	65, 70, 68, 26, 46
LDEDBO	1588.0	0.9481	00:00–04:00	69, 70, 71, 72, 73
			05:00–11:00	69, 70, 14, 53, 46
			12:00–14:00	10, 70, 71, 72, 47
			15:00–19:00	69, 70, 71, 49, 38
			20:00–24:00	69, 70, 71, 72, 46

Table 9. GA, PSO, DBO and LDEDBO multi-period dynamic reconfiguration analyses of IEEE-69 medium-scale node bus.

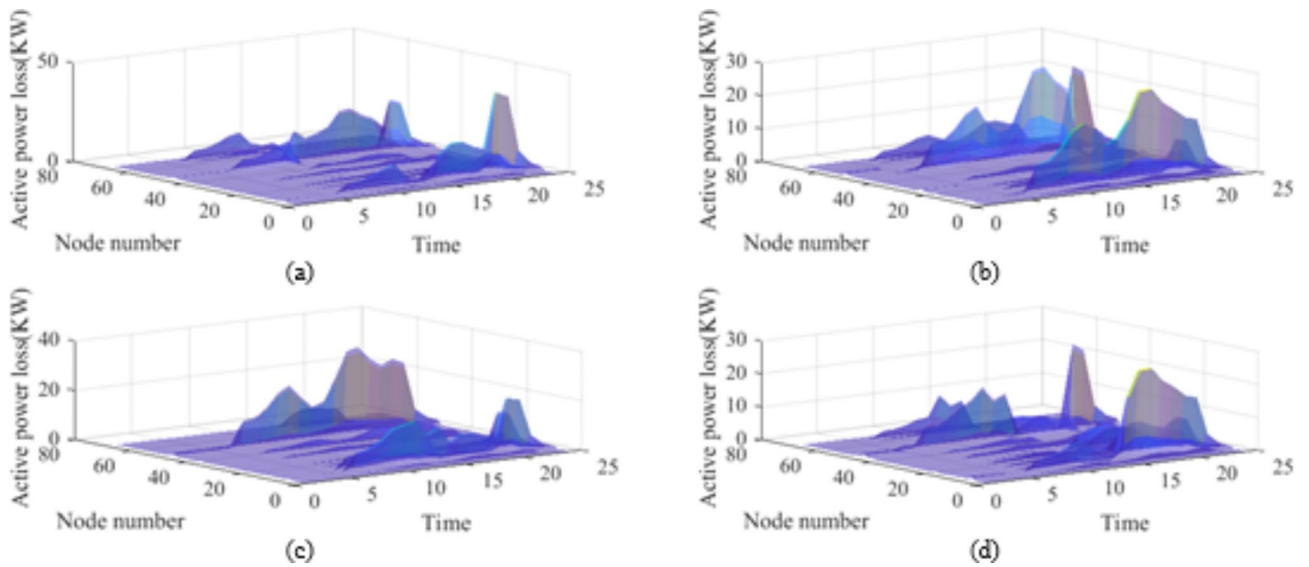


Fig. 14. Active power dissipation of IEEE-69 medium-scale node bus in 24 h: (a) GA; (b) PSO; (c) DBO; (d) LDEDBO.

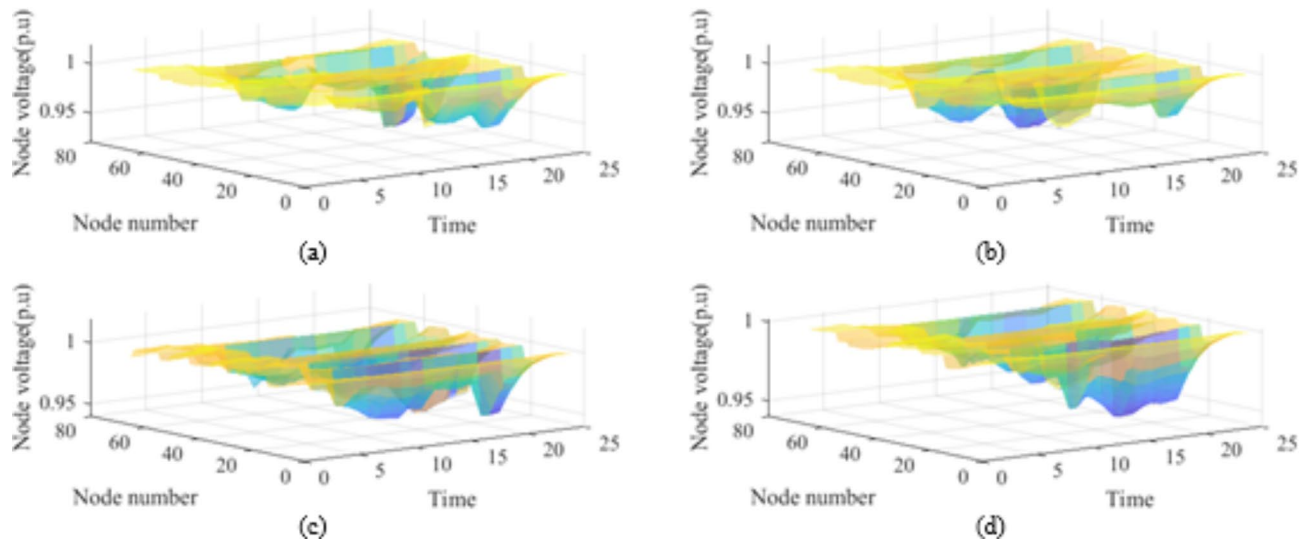


Fig. 15. Voltage fluctuation of IEEE-69 medium-scale node bus in 24 h: (a) GA; (b) PSO; (c) DBO; (d) LDEDDBO.

Data availability

All data included in this study are available upon request by contact with the corresponding author.

Received: 3 July 2024; Accepted: 13 December 2024

Published online: 28 December 2024

References

1. Wiatros-Motyka, M. Global Power Review EMBER. <https://ember-climate.org/insights/research/global-electricity-review-2023/> (2023).
2. Bui, V. H. & Su, W. Real-time operation of distribution network: A deep reinforcement learning-based reconfiguration approach. *Sustain. Energy Technol. Assess.* **50**, 101841 (2022).
3. Ahmadi, H. & Marti, J. R. Distribution system optimization based on a linear power-flow formulation. *IEEE Trans. Power Deliv.* **30**, 25–33 (2015).
4. Azad-Farsani, E., Sardou, I. G. & Abedini, S. Distribution Network Reconfiguration based on LMP at DG connected buses using game theory and self-adaptive FWA. *Energy* **215**, 119146 (2021).
5. Chandramohan, S., Atturulu, N., Devi, R. P. K. & Venkatesh, B. Operating cost minimization of a radial distribution system in a deregulated electricity market through reconfiguration using NSGA method. *Int. J. Electr. Power Energy Syst.* **32**, 126–132 (2010).
6. Gözel, T. & Hocaoglu, M. H. An analytical method for the sizing and siting of distributed generators in radial systems. *Electr. Power Syst. Res.* **79**, 912–918 (2009).
7. Gupta, N., Swarnkar, A. & Niazi, K. R. Distribution network reconfiguration for power quality and reliability improvement using Genetic Algorithms. *Int. J. Electr. Power Energy Syst.* **54**, 664–671 (2014).
8. Hamour, H. et al. and Distribution network reconfiguration using grasshopper optimization algorithm for power loss minimization. In *International Conference on Smart Energy Systems and Technologies (SEST)*. (2018).
9. Hui, W. et al. In *The 27th Chinese Control and Decision Conference* 1243–1247 (CCDC, 2015).
10. Jafar-Nowdeh, A. et al. Meta-heuristic matrix moth-flame algorithm for optimal reconfiguration of distribution networks and placement of solar and wind renewable sources considering reliability. *Environ. Technol. Innov.* **20**, 101118 (2020).
11. Young-Jae, J., Jae-Chul, K., Jin, O. K., Joong-Rin, S. & Lee, K. Y. An efficient simulated annealing algorithm for network reconfiguration in large-scale distribution systems. *IEEE Trans. Power Deliv.* **17**, 1070–1078 (2002).
12. Kovački, N. V., Vidović, P. M. & Sarić, A. T. Scalable algorithm for the dynamic reconfiguration of the distribution network using the Lagrange relaxation approach. *Int. J. Electr. Power Energy Syst.* **94**, 188–202 (2018).
13. Xu, T. et al. Multi-objective robust optimization of active distribution networks considering uncertainties of photovoltaic. *Int. J. Electr. Power Energy Syst.* **133**, 107197 (2021).
14. Pan, J. S., Wang, H. J., Nguyen, T. T., Zou, F. M. & Chu, S. C. Dynamic reconfiguration of distribution network based on dynamic optimal period division and multi-group flight slime mould algorithm. *Electr. Power Syst. Res.* **208**, 107925 (2022).
15. Wang, J., Wang, W., Yuan, Z., Wang, H. & Wu, J. A. Chaos disturbed beetle antennae search algorithm for a multiobjective distribution network reconfiguration considering the variation of load and DG. *IEEE Access.* **8**, 97392–97407 (2020).
16. Li, L. L., Xiong, J. L., Tseng, M. L., Yan, Z. & Lim, M. K. Using multi-objective sparrow search algorithm to establish active distribution network dynamic reconfiguration integrated optimization. *Expert Syst. Appl.* **193**, 116445 (2022).
17. Senapati, M. K. & Khamari, R. C. Improving power quality with intelligent control. *J. Electr. Syst.* **20** (10s), pp3118–3130 (2024).
18. Senapati, M. K., Pradhan, C., Samantaray, S. R. & Nayak, P. K. Improved power management control strategy for renewable energy-based DC micro-grid with energy storage integration. *IET Gener. Transm. Distrib.* **13**, 838–849 (2019).
19. Senapati, M. K., Pradhan, C. & Calay, R. K. A computational intelligence based maximum power point tracking for photovoltaic power generation system with small-signal analysis. *Optimal Control Appl. Methods.* **44**, 617–636 (2023).
20. Senapati, M. K. et al. Advancing electric vehicle charging ecosystems with intelligent control of DC microgrid stability. *IEEE Trans. Ind. Appl.* **60**, 7264–7278 (2024).
21. Wang, C., Gu, J., Sun, W., Mou, H. & Naiyuan, X. In *2015 11th International Conference on Natural Computation (ICNC)* 1285–1289 (2015).
22. Wu, Y., Liu, J., Wang, L., An, Y. & Zhang, X. Distribution network reconfiguration using chaotic particle swarm chicken swarm fusion optimization algorithm. *Energies* **24**, 3251–3259 (2024).

23. Rao, R. S., Narasimham, S. V. L., Raju, M. R. & Rao, A. S. Optimal network reconfiguration of large-scale distribution system using harmony search algorithm. *IEEE Trans. Power Syst.* **26**, 1080–1088 (2011).
24. Hamour, H., Kamel, S., Abdel-mawgoud, H., Korashy, A. & Jurado, F. In *2018 International Conference on Smart Energy Systems and Technologies (SEST)* 1–5 (2018).
25. Mirjalili, S., Mirjalili, S. M. & Lewis, A. Grey wolf optimizer. *Adv. Eng. Softw.* **69**, 46–61 (2014).
26. Mirjalili, S. Moth-flame optimization algorithm: A novel nature-inspired heuristic paradigm. *Knowl. Based Syst.* **89**, 228–249 (2015).
27. Mirjalili, S. & Lewis, A. The whale optimization algorithm. *Adv. Eng. Softw.* **95**, 51–67 (2016).
28. Shaheen, A. M., El-Sehiemy, R. A. & Farrag, S. M. In *2018 International Conference on Innovative Trends in Computer Engineering (ITCE)* 344–349 (2018).
29. Xue, J. & Shen, B. Dung beetle optimizer: a new meta-heuristic algorithm for global optimization. *J. Supercomput.* **79**, 7305–7336 (2023).
30. Sultana, B., Mustafa, M. W., Sultana, U. & Bhatti, A. R. Review on reliability improvement and power loss reduction in distribution system via network reconfiguration. *Renew. Sustain. Energy Rev.* **66**, 297–310 (2016).
31. Nguyen, T. T., Nguyen, T. T., Truong, A. V., Nguyen, Q. T. & Phung, T. A. Multi-objective electric distribution network reconfiguration solution using runner-root algorithm. *Appl. Soft Comput.* **52**, 93–108 (2017).
32. Alghafri, M., Alghazi, A., Almoghathawi, Y., Saleh, H. & Al-Shareef, K. Smart City Charging Station allocation for electric vehicles using analytic hierarchy process and multiobjective goal-programming. *Appl. Energy*. **372**, 123775 (2024).
33. Senapati, M. K. & Sarangi, S. Secured zone 3 protection during load encroachment using synchrophasor data. *Sustainable Energy Grids Networks*. **27**, 100522 (2021).
34. Slowik, A. & Kwasnicka, H. Evolutionary algorithms and their applications to engineering problems. *Neural Comput. Appl.* **32**, 12363–12379 (2020).

Author contributions

Conceptualization, Y.W., L.W. and Z.W.; Methodology, Y.W. and L.W.; Software, Y.W. and L.W.; Validation, L.W., J.L. and Y.W.; Formal analysis, L.W., J.L. and Y.W.; Investigation, Y.W.; Data curation, L.W.; Writing—original draft, Y.W., and L.W.; Writing—review & editing, Y.W., L.W., Y.A. and X.Z.; Visualization, Y.W.; Supervision, L.W.; Funding acquisition, Y.W. and D.F.

Declarations

Competing interests

The authors declare no competing interests.

Additional information

Supplementary Information The online version contains supplementary material available at <https://doi.org/10.1038/s41598-024-83307-5>.

Correspondence and requests for materials should be addressed to L.W.

Reprints and permissions information is available at www.nature.com/reprints.

Publisher's note Springer Nature remains neutral with regard to jurisdictional claims in published maps and institutional affiliations.

Open Access This article is licensed under a Creative Commons Attribution-NonCommercial-NoDerivatives 4.0 International License, which permits any non-commercial use, sharing, distribution and reproduction in any medium or format, as long as you give appropriate credit to the original author(s) and the source, provide a link to the Creative Commons licence, and indicate if you modified the licensed material. You do not have permission under this licence to share adapted material derived from this article or parts of it. The images or other third party material in this article are included in the article's Creative Commons licence, unless indicated otherwise in a credit line to the material. If material is not included in the article's Creative Commons licence and your intended use is not permitted by statutory regulation or exceeds the permitted use, you will need to obtain permission directly from the copyright holder. To view a copy of this licence, visit <http://creativecommons.org/licenses/by-nc-nd/4.0/>.

© The Author(s) 2024